JOURNAL OF GEOPHYSICAL RESEARCH, VOL. 114, D01202, doi:10.1029/2008JD010579, 2009

Solar zenith and viewing geometry-dependent errors in satellite retrieved cloud optical thickness: Marine stratocumulus case

Seiji Kato[1] and Alexander Marshak[2]

Received 10 June 2008; revised 17 September 2008; accepted 9 October 2008; published 3 January 2009.

[1] The error in the domain-averaged cloud optical thickness retrieved from satellite-based imagers is investigated using a cloud field generated by a cloud model and a 3D radiative transfer model. The objective of this study is to identify the optimal geometry for the optical thickness retrieval and quantify the error. The cloud field used in the simulation is a relatively uniform (retrieved shape parameter of a gamma distribution averaged over all simulated viewing and solar zenith angles is 18) and nearly isotropic stratocumulus field. The retrieved cloud cover with a 1-km pixel resolution is 100%. The domain-averaged optical thickness error is separated into two terms, the error caused by an assumption of a horizontally uniform cloud over a 1-km pixel (internal variability) and error caused by neglecting the horizontal flux through the boundary of subpixels (external variability). For the cloud field used in this study, the external variability term increases with solar zenith angle and the sign changes from negative to positive while the internal variability term is generally negative and becomes more negative as the solar zenith angle increases. At a small solar zenith angle, therefore, both terms are negative, but the error partially cancels at a large solar zenith angle. When the solar zenith angle is less than 30°, both terms are small; the error in the viewing zenith angle and domain-averaged cloud optical thickness derived from the relative azimuth angle smaller than 150 is less than 10%. However, if the optical thickness is derived from nadir view only for overhead sun, the domain-averaged optical thickness is underestimated by more than 10%. When the solar zenith angle increases to 60°, the internal variability term exceeds 10%, especially viewed from the forward direction, but the domain and viewing zenith angle averaged optical thickness error can be less than 10% in the backward direction. When the solar zenith angle is 70°, both terms are greater than 10%. The shape parameter of a gamma distribution derived from retrieved optical thicknesses increases with the viewing zenith angle but decreases with solar zenith angle. On the basis of this simulation and Terra Moderate Resolution Imaging Spectroradiometer (MODIS) viewing geometry and solar zenith angle at the sampling time over the northeastern Pacific, the error in the domain-averaged retrieved optical thickness of uniform stratocumulus over northeastern Pacific is less than 10% in March and September.

Citation: Kato, S., and A. Marshak (2009), Solar zenith and viewing geometry-dependent errors in satellite retrieved cloud optical thickness: Marine stratocumulus case, *J. Geophys. Res.*, *114*, D01202, doi:10.1029/2008JD010579.

1. Introduction

[2] Clouds reduce the global radiation budget [*Ramanathan et al.*, 1989], increase its interannual variability (S. Kato, Interannual variability of global radiation budget, 2008, submitted to *Journal of Climate*, 2008, hereinafter referred to as Kato, submitted manuscript, 2008) and play a key role in climate feedback processes. Understanding their spatial and temporal variabilities as a function of key meteorological variables is essential in modeling their response to and understanding their role in climate change. Observationally, global cloud properties can be estimated only by satellite-based instruments. Among cloud properties, cloud cover contributes most to the global top-of-atmosphere (TOA) irradiance variability [*Loeb et al.*, 2007; Kato, submitted manuscript, 2008]. The cloud optical thickness is the most important of all cloud optical properties, and vital for any cloud-radiation parameterization. Its impact on radiative fluxes and therefore on climate is exceeded only by cloud cover. It is also the entry point of other retrieved cloud properties such as droplet size, liquid water and ice water contents [e.g., *Minnis et al.*, 1998; *Platnick et al.*, 2001] because the retrieval of these properties requires the optical thickness. Therefore understanding the

[1]Climate Directorate, NASA Langley Research Center, Hampton, Virginia, USA.
[2]Climate and Radiation Branch, NASA Goddard Space Flight Center, Greenbelt, Maryland, USA.

possible error in the satellite-derived cloud optical thickness is essential for assessing the error in climate data sets.

[3] Besides imager calibration drifts and uncertainties in surface albedo and atmospheric correction, the error in satellite-derived cloud optical thickness depends on cloud type, illumination and viewing geometry: solar zenith angle, viewing zenith and relative azimuth angles. Comparing 2D and independent column approximation (ICA), it was found [e.g., *Chambers et al.*, 1997; *Zuidema and Evans*, 1998] that the retrieved optical thickness is smaller than the true optical thickness when the sun is overhead. In contrast, for oblique illumination, the retrieved optical thickness can be larger than the true one. The retrieved optical thickness from horizontally inhomogeneous clouds decreases with increasing the imager pixel size [*Zuidema and Evans*, 1998]. *Várnai and Marshak* [2003] used both 3D and ICA to understand the mechanism causing the reflectance difference at nadir. They showed that, when the solar zenith angle is 60, the nadir view 3D reflectance is typically larger than reflectance computed with ICA because the nadir view reflectance is enhanced by less scattering events in 3D than in ICA caused by side illumination of clouds in 3D.

[4] Because the error in the retrieved cloud optical thickness depends on other cloud properties, it is difficult to understand the error by analyzing satellite-derived cloud optical thicknesses, although the error can be addressed through analyses of viewing angle dependence of retrieved optical thickness [e.g., *Loeb et al.*, 1997; *Loeb and Coakley*, 1998; *Várnai and Marshak*, 2007]. Surface-based and in-situ measurements can provide data for validation [e.g., *Mace et al.*, 2005; *Dong et al.*, 2008], but the field-of-view difference adds a complication in understanding the accuracy of retrievals. Another, somewhat less utilized, way to understand the error in the retrieved cloud optical thickness is by simulating the retrieval process with realistic cloud fields. In this approach, clouds fields were obtained in several different ways. For example, *Zuidema and Evans* [1998] retrieved cloud fields from a ground-based radar and a microwave radiometer, *Kato et al.* [2006] used cloud fields generated by a cloud model, and *Zinner and Mayer* [2006] obtained the 3d cloud structure from airborne radiance observations using a retrieval technique developed by *Zinner et al.* [2006]. The advantage of this approach is that the true cloud optical thickness is known and the exact error can be accurately estimated. The disadvantage is that it is unknown how well cloud fields used in the study represent real cloud fields. As a consequence, the result derived from simulations using a particular cloud field may not be directly applied to other cloud fields. However, if we are able to identify a viewing geometry that gives the smallest optical thickness retrieval error, we have a better chance of understanding the possible error when we analyze the viewing zenith and relative azimuth angle dependence of retrieved optical thicknesses. Therefore the purpose of this paper is to understand solar zenith, viewing zenith, and relative azimuth angle-dependent error in the optical thickness retrieved from relatively uniform low-level water clouds simulated with a cloud resolving model [*Stevens et al.*, 1999].

[5] Instead of analyzing the error in the retrieved optical thickness from individual pixels, we will be focusing on the error in domain-averaged retrieved optical thicknesses as a function of the imager viewing geometry and solar zenith angle in this study. Investigating domain-averaged errors instead of pixel-by-pixel errors makes the analysis less complicated because errors often partially cancel each other in an averaging process. In addition, understanding the error in the domain-averaged optical thickness is more practical because averaged properties, such as regional, zonal, daily, or monthly means, are used to investigate climate problems.

[6] We investigate the error as a function of viewing zenith, relative azimuth and solar zenith angles to answer three questions: (1) what is the optimal condition of the viewing, relative azimuth, and solar zenith angles in retrieving optical thickness from satellite-based imagers for relatively uniform water clouds over ocean, (2) whether or not the optimal geometry gives a sufficiently small error for climate analyses, and (3) accounting for satellite and solar geometry, how accurate are the Moderate Resolution Imaging Spectroradiometer (MODIS [*King et al.*, 1992]) retrievals of cloud optical thickness for stratocumulus over ocean? Our emphasis is on identifying the optimal geometry that gives sufficiently small error in retrieved optical thicknesses instead of pointing out a large error in them.

[7] In this study, we limit the analysis to the errors caused by a uniform overcast plane parallel cloud over an imager pixel and the independent column approximation (ICA). Therefore our error analysis does not account for the uncertainty in the surface bidirectional reflectance function and atmospheric extinction above and below clouds.

[8] In the following section, after a brief description of the cloud field (section 2), we start with separating the error into two terms in section 3 and focus on the difference in the radiance computed with ICA and full 3D in section 4. Section 5 analyzes the error by viewing geometry and solar zenith angle and seeks for an optimal viewing geometry. Section 6 investigates whether or not the optimal viewing geometry actually occurs in the data taken by MODIS on Terra over regions where low-level water clouds are often present.

2. Method

[9] A cloud field of stratocumulus in a marine boundary layer with domain-averaged optical thickness of 3.75 (Table 1) was generated by a cloud resolving model [*Stevens et al.*, 1999] and described in the study by *Kato et al.* [2006, ASTEX-Sc]. The horizontal resolution of the modeled liquid water content field is 50 m and the domain size is 3.4 km by 3.4 km. The vertical resolution is 25 m and the total number of vertical layers is 13. The threshold of liquid water content is set to give the cloud fraction of 0.96 over the domain but the retrieved cloud fraction with 1-km pixels is 1. With this cloud field, we simulate a satellite-based cloud optical thickness retrieval process from narrowband visible radiances. Clouds are non-absorbing and the droplet effective radius is assumed to be 10 μm everywhere. The albedo of the underlying surface is 0.05, which is a typical value for an ocean surface in a visible wavelength. We use the Spherical Harmonics Discrete Ordinate Method (SHDOM [*Evans*, 1998]) to compute radiances.

[10] As indicated in Table 1 in the study by *Kato et al.* [2006], the cloud field used in this study is not isotropic because the cloud field vertically tilts toward the direction

Table 1. Model Generated Cloud Properties

Mean optical thickness	3.75
Shape parameter (ν) (1 km resolution)	14.9
Cloud fraction (50-m resolution)	0.960
Domain size (km)	3.4 × 3.4

of wind shear [*Hinkelman et al.*, 2005]. In other words, the radiance computed with a full 3D mode is a function of orientation of the cloud field relative to the sun position in addition to the viewing θ, relative azimuth ϕ, and solar zenith angles θ_0. Note that the relative azimuth angle is 0 when the imager views toward the sun position. The error in actual retrieved cloud optical thicknesses from imagers also depends on both the viewing geometry and cloud field orientation relative to the sun position. However, if clouds do not have a systematic orientation relative to the sun, we expect that the dependence to the cloud field orientation affecting optical thickness retrievals becomes negligible when many retrieved optical thicknesses are averaged, as if the domain-averaged cloud optical thickness is derived from isotropic cloud fields. The indication of apparent isotropic cloud fields in actual satellite data is that retrieved optical thicknesses sorted by viewing and relative azimuth angles is nearly symmetric about the principal plane if the temporal sampling among angles is uniform. Hence we assume that there is no preferential cloud field orientation relative to the sun position in domain-averaged data. The error in retrieved cloud optical thicknesses is, therefore, only a function of viewing zenith, relative azimuth, and solar zenith angles. To minimize the effect of anisotropic cloud fields, we rotate the original cloud field by 180°. We compute the reflectance at 7 relative azimuth angles with an increment of 30° from 0° through 180° for both the original and 180° rotated cloud field. We then average the reflectance pair of each relative azimuth angle.

[11] The reflectance from an individual pixel observed by an imager does not obey the reciprocity principle because photons incident on the outside of the pixel affect the radiance observed from the pixel [e.g., *Davies*, 1994; *Aronson*, 1997; *Di Girolamo et al.*, 1998]. However, under a periodic boundary condition, which does not have net photon transport through the boundary of the domain, the domain-averaged reflectance is supposed to obey the reciprocity principle [*Di Girolamo*, 2002; *Davis and Knyazikhin*, 2005]. Two reciprocal pairs of the reflectance in our simulation, even when the cloud field orientation relative to the sun is considered, are (30°, 0°, 60°) and (60°, 0°, 30°); (30°, 180°, 60°) and (60°, 180°, 30°), where angles in the parenthesis are (θ, ϕ, θ_0). In addition, if the cloud field is isotropic, the reflectance is symmetric around the principal plane so that more reciprocal pairs are possible. These reciprocal pairs that should obey the reciprocity principle, if the radiance is symmetric around the principal plane, are also listed in Table 2. The largest reflectance relative difference among these reciprocal pairs is 2.7%. Although we only average two radiation fields by rotating the cloud field by 180°, Table 2 indicates that the effect of anisotropic cloud field in averaged radiation fields is small. Because of this, the viewing zenith angle and solar zenith angle are interchangeable for the azimuthally averaged domain average reflectance from the simulation.

[12] In this studies, we define the reflectance r as

$$r = \frac{\pi I}{\cos\theta_0 F_0}, \tag{1}$$

where θ_0 is the solar zenith angle, I is the radiance, and F_0 is the solar constant of the narrowband wavelength.

3. Optical Thickness Error

[13] To better understand causes of the error in the domain-averaged retrieved cloud optical thicknesses, we split it into two parts as follows:

$$\overline{\Delta\tau} = \overline{\tau_{3D,1km}} - \overline{\tau_{true}} = \left(\overline{\tau_{3D,1km}} - \frac{1}{N}\sum_{j=1}^{N}\tau_{3D,50m,j}\right) + \left(\frac{1}{N}\sum_{j=1}^{N}\tau_{3D,50m,j} - \overline{\tau_{true}}\right) = \overline{\Delta\tau_i} + \overline{\Delta\tau_e}, \tag{2}$$

where $\overline{\tau_{3D,1km}}$ is the domain-averaged optical thickness retrieved from the 3D 1-km resolution reflectance r_{3D}, $\overline{\tau_{true}}$ is the true domain-averaged optical thickness, $\tau_{3D,50m,j}$ is the subpixel optical thickness retrieved from a subpixel (50 m in our case) 3D reflectance r_j; N is the total number of cloudy subpixels and finally, $\overline{\Delta\tau_i}$ and $\overline{\Delta\tau_e}$ stand for the error due to the internal and external variability, respectively. The plane-parallel assumption of an uniform homogeneous cloud over the 1-km pixel is responsible for the first term $\overline{\Delta\tau_i}$, while the application of the ICA to 50 m subpixels is responsible for the second term $\overline{\Delta\tau_e}$ [see *Cahalan et al.*, 1994]. Therefore, $\overline{\Delta\tau_e}$ represents the domain averaged error in the optical thickness retrieval at a 50 m resolution. Because of a use of a moving window centered at each grid point, the total number of 1 km × 1 km pixels is

Table 2. 3D Reflectance at Reciprocity Angles

Angle (θ, ϕ, θ_0)	3D Reflectance	Relative Difference (%)
(30, 0, 60)	0.2519	
(60, 0, 30)	0.2506	0.5
(30, 180, 60)	0.2671	
(60, 180, 30)	0.2665	0.2
(30, any, 0)	0.1838	
(0, any, 30)	0.1845	0.4
(60, any, 0)	0.1764	
(0, any, 60)	0.1799	2.0
(30, 30, 60)	0.2386	
(60, 30, 30)	0.2355	1.3
(30, 60, 60)	0.2151	
(60, 60, 30)	0.2107	2.1
(30, 90, 60)	0.2031	
(60, 90, 30)	0.1981	2.5
(30, 120, 60)	0.2145	
(60, 120, 30)	0.2088	2.7
(30, 150, 60)	0.2784	
(60, 150, 30)	0.2749	1.3

equal to 4624, which is equal to the total number of 50 m × 50 m pixels.

[14] Considering that the external variability term $\overline{\Delta\tau_e}$ is caused by the ICA and using Taylor expansion at each pixel, we can write as follows,

$$\frac{1}{N}\sum_{j=1}^{N}\tau_{3D,\ 50\ m,\ j} \approx \overline{\tau_{true}} - \frac{1}{N}\sum_{j=1}^{N}(r_{ICAj} - r_{3Dj})\frac{\partial\tau}{\partial r_{ICA\,j}}, \qquad (3)$$

where r_{ICA} is the reflectance computed with the ICA. Since $\frac{\partial\tau}{\partial r_{ICA}}$ increases as a function of r, the difference between r_{3D} and r_{ICA} at pixels with larger optical thicknesses contributes to $\overline{\Delta\tau_e}$ more than the difference at pixels with smaller optical thicknesses if the magnitude of $r_{3D} - r_{ICA}$ is the same. Understanding the difference between $\overline{r_{ICA}}$ and $\overline{r_{3D}}$ is the first step to understand $\overline{\Delta\tau_e}$ because the derivative of the optical thickness with respect to reflectance is known. For the comparison, both r_{ICA} and r_{3D} need to be at a same resolution for the following reason. It is well known that for horizontally inhomogeneous clouds [e.g. *Marshak et al.*, 2006],

$$\overline{r(\tau)} < r(\bar{\tau}), \qquad (4)$$

because the reflected radiance $r(\tau)$, as a function of optical thickness τ, is a convex function. Therefore, if the resolution of r_{ICA} is coarse and the optical thickness is linearly averaged to compute the domain averaged reflectance, $r_{ICA}(\tau)$ with a coarse resolution is greater than $r_{ICA}(\tau)$ with a finer resolution. To separate the errors clearly, both r_{3Dj} and r_{ICAj} are computed for each pixel at the 50 m cloud model resolution. The optical thickness is then retrieved from 50 m resolution radiances. In the following section, we investigate $\overline{\Delta\tau_e}$ by analyzing the difference between $\overline{r_{3D}}$ and $\overline{r_{ICA}}$.

4. ICA and 3D Reflectance Difference

[15] Figure 1 shows the domain-averaged reflectance difference $\overline{r_{ICA}} - \overline{r_{3D}} = \overline{\Delta r_{ICA}}$ as a function of relative azimuth angle for different viewing zenith and solar zenith angles. Each point is the average of 9248 (68 × 68 × 2) differences of 1-km reflectances except for nadir view with overhead sun (4624 differences). Prominent features in Figure 1 are:

[16] 1. The nadir view reflectance difference $\overline{\Delta r_{ICA}}$ decreases with increasing solar zenith angle (except near overhead sun).

[17] 2. In the forward direction ($\phi < 90°$), $\overline{\Delta r_{ICA}}$ at large ($\theta \geq 60°$) and small ($\theta \leq 30°$) viewing zenith angle show different solar zenith angle dependence: it decreases with solar zenith angle at small viewing zenith angles while it increases at large viewing zenith angles (except near overhead sun). In the backward direction ($\phi > 90°$) $\overline{\Delta r_{ICA}}$ decreases with solar zenith angle (except near overhead sun) for all viewing zenith angles.

[18] 3. At large viewing and solar zenith angles, $\overline{\Delta r_{ICA}}$ is positive in the forward direction and negative in the backward direction, monotonically decreasing with increasing relative azimuth angle.

[19] 4. The root-mean-square (RMS) $r_{ICA} - r_{3D}$ difference increases with solar zenith angle for all viewing zenith angles and with viewing zenith angle for all solar zenith angles.

[20] 5. The RMS $r_{ICA} - r_{3D}$ difference is smallest when clouds are viewed from relative azimuth angle near 90 for a large viewing zenith angle.

[21] Note that the distinction between large and small angles are somewhat arbitrary but a dramatic difference between the second and third rows on the left column in Figure 1 indicates that 30° is considered to be a small angle and 60° is considered to be a large angle.

[22] In Figure 2, the $\overline{\Delta r_{ICA}}$ from all azimuth angles are averaged and the difference is plotted as a function of viewing zenith angle (open circles). Applying the reciprocity principle, we also plot additional points (open squares). As mentioned earlier, azimuthally and domain-averaged reflectance difference $\overline{\Delta r_{ICA}}$ obeys the reciprocity principle fairly well, which is a result of a nearly isotropic cloud field and a periodic boundary condition.

[23] In this section, we examine the cause of the above features and investigate the reasons for the $\overline{r_{ICA}} - \overline{r_{3D}}$ difference. For overhead sun and a small viewing zenith angle, $\overline{r_{ICA}}$ is larger than $\overline{r_{3D}}$. When the solar zenith angle is small, photons leaks from the side of clouds in 3D computations while photons leave clouds only from top or bottom with ICA. Side leakage, however, does not necessarily mean that $\overline{r_{ICA}}$ at nadir is larger than $\overline{r_{3D}}$ because understanding the reflectance difference requires to know the direction in which photons leave. A larger $\overline{r_{ICA}}$ at nadir implies that photons are reflected toward a smaller zenith angle with ICA than the 3D computation when the sun is overhead. Because cloud droplets scatter photons predominately in forward direction, photons reflected near nadir directions tend to have experienced more scattering events than those reflected at oblique angles for overhead sun. Using a Monte Carlo simulation, Figure 3 shows that, for overhead sun, photons reflected in nadir direction experience more scattering events than those reflected oblique angles. A larger $\overline{r_{ICA}}$ than $\overline{r_{3D}}$ near nadir for overhead sun, therefore, can be attributed to the difference in the number of scattering events, that is, the ICA tends to increase the number of scattering events compared with 3D computations. Note that slopes of the number of scattering events versus optical thickness in Figure 3 are approximately 1 as explained from the diffusion theory [*Marshak et al.*, 1995]. When the reciprocity principal is applied, a smaller $\overline{r_{ICA}}$ than $\overline{r_{3D}}$ at oblique viewing angles for overhead sun is equivalent to a larger $\overline{r_{3D}}$ than $\overline{r_{ICA}}$ near nadir when the solar zenith angle is large. In addition, together with the above result of $\overline{\Delta r_{ICA}}$ for overhead sun, it follows that $\overline{\Delta r_{ICA}}$ at nadir decreases with solar zenith angle.

[24] When the solar zenith angle is large, $\overline{\Delta r_{ICA}}$ is more dependent on relative azimuth angle and relative azimuth angle dependence of $\overline{\Delta r_{ICA}}$ increases as the viewing zenith angle increases. In the forward direction where the imager detects transmitted photons and could see shadows, r_{ICA} is larger than r_{3D}. In the backward direction, the effect tends to be opposite because the imager views sunlit areas that are closer to perpendicular to direct solar radiation in 3D computations than with ICA. This effect is further pronounced when the actual cloud fraction is less than 1 (e.g.,

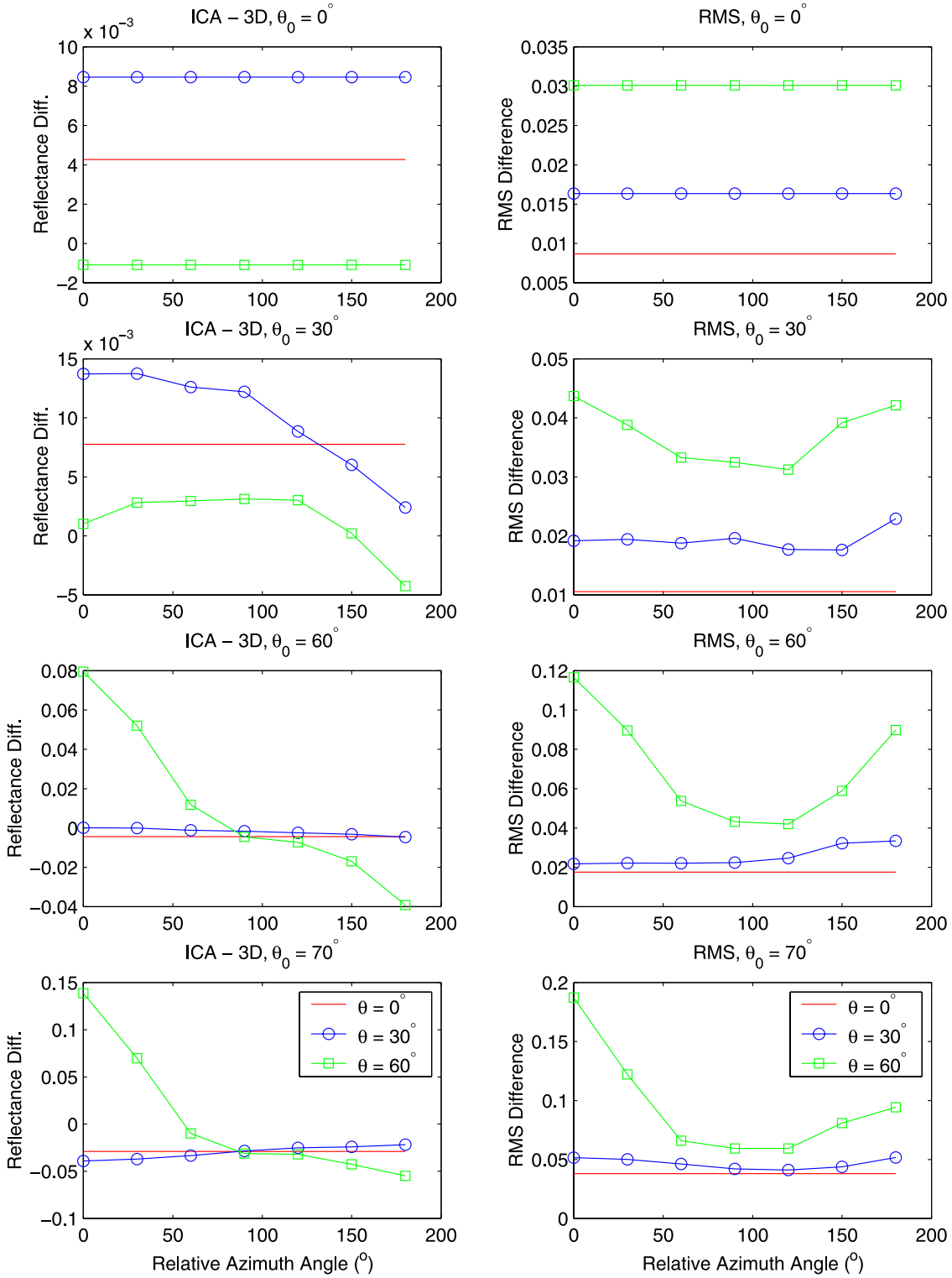

Figure 1. (left) Difference of the domain-averaged reflectance computed with the independent column approximation (ICA) from 3D reflectance as a function of relative azimuth angle. The relative azimuth angle is 0 when the imager looks into the sun. (right) Root-mean-square difference of the ICA and 3D reflectance. ICA and 3D reflectances are computed with a 50-m resolution. Solid lines indicate nadir view, and lines with open circles and squares indicate, respectively, the viewing zenith angle of 30° and 60°. The solar zenith angle increases from the top to bottom row (0°, 30°, 60°, and 70°).

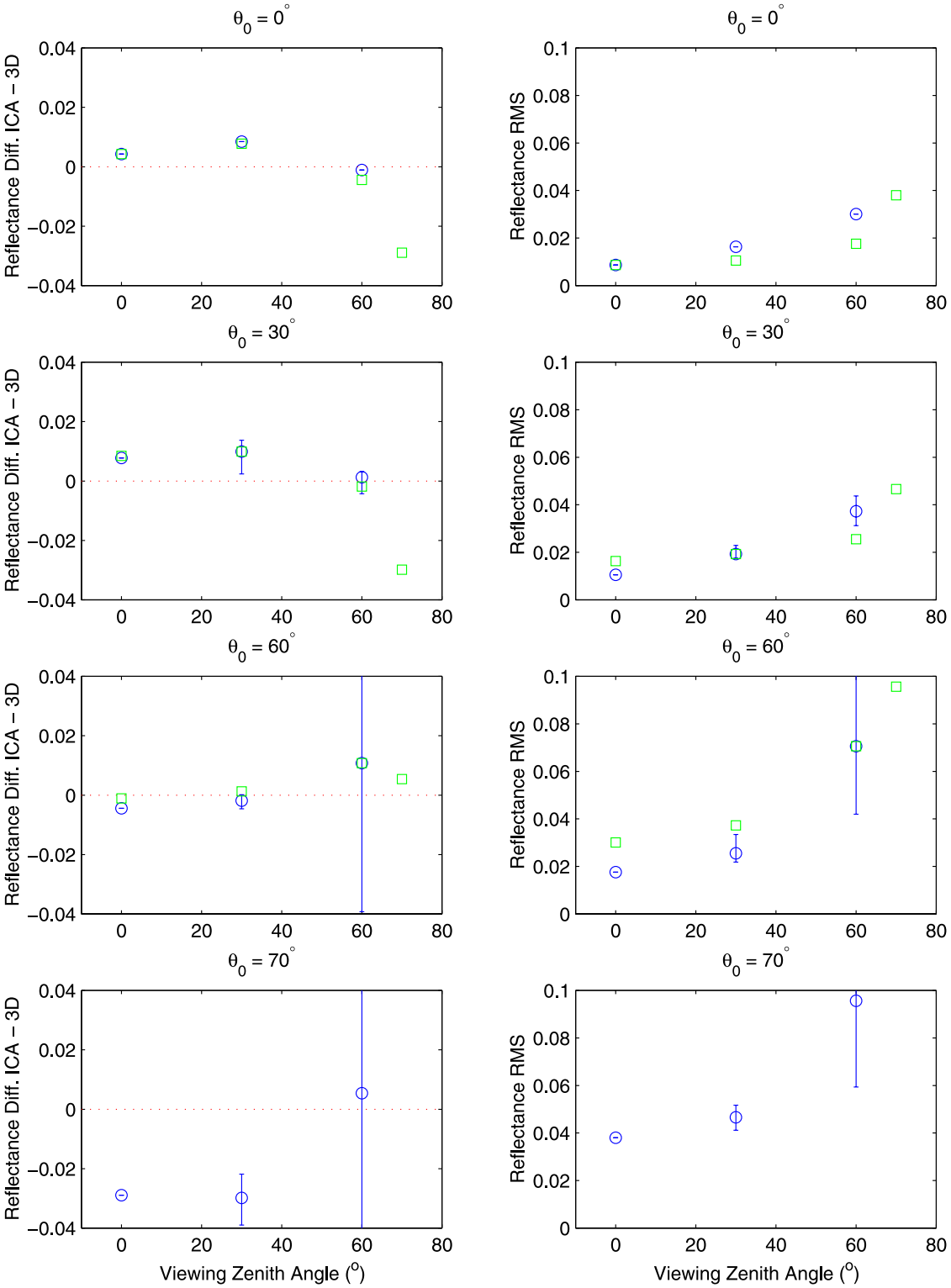

Figure 2. (left) Difference of the azimuthally and domain-averaged reflectance computed with the independent column approximation (ICA) from 3D reflectance as a function of viewing zenith angle (open circles). Reflectances at 7 different relative azimuth angles shown in Figure 1 are averaged for each point. The error bar indicates the maximum and minimum reflectances among different relative azimuth angles. (right) Same as Figure 2 (left) but for root-mean-square difference of ICA and 3D radiances. Values indicated by open squares are obtained with the reciprocity principle (i.e., with interchanging solar and viewing zenith angles).

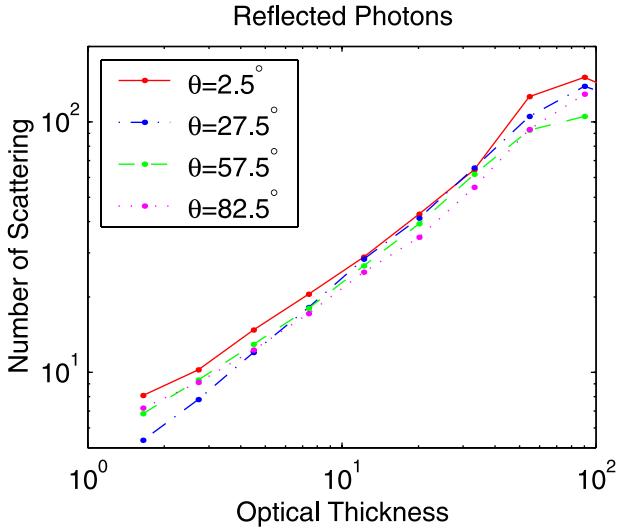

Figure 3. Number of scattering events as a function of optical thickness for reflected photons for overhead sun. The cloud is plane parallel and non-absorbing. The asymmetry parameter of cloud droplet is 0.86, and the Henyey-Greenstein phase function is used. Different lines are for different viewing zenith angles indicated in the legend.

the true cloud fraction is 0.96 for the cloud field used in this study), especially near 180° relative azimuth angle because the cloud fraction projected in the direction of direct solar radiation increases with solar zenith angle in 3D computation while it is constant with ICA.

[25] In summary, the ICA tends to increase the number of scattering events compared with 3D computations. As a consequence, $\overline{r_{ICA}}$ is larger than $\overline{r_{3D}}$ at nadir for overhead sun and the difference decreases with viewing zenith angle. Applying the reciprocity principal, this viewing zenith angle dependence of the difference for overhead sun is equivalent to decreasing $\overline{\Delta r_{3D}}$ at the nadir with increasing solar zenith angle. We can interpret the increase of the number of scattering events by the ICA as a larger apparent optical thickness in ICA computations. However, a simple correction to the optical thickness to match $\overline{r_{ICA}}$ with $\overline{r_{3D}}$ for all angles does not exist because the adjustment of $\Delta\tau$ depends on the viewing zenith angle for a given number of scattering events increase determine by the cloud field.

[26] The sensitivity of viewing zenith dependence of number of scattering events to cloud top structure is weak, which is apparent in the study by *Loeb et al.* [1998] who analyzed the number of scattering events as a function of viewing zenith angle using various cloud top boundaries. Their result indicates that the difference in the number of scattering events between 3D and 1D computations is smaller than the difference caused by the viewing zenith angle. Therefore the mean number of scattering events for a given direction is less sensitive to cloud top variability than to viewing zenith angle, except in the forward direction when the solar zenith angle is large.

[27] Briefly, we consider whether or not above results are consistent with earlier result of the irradiance difference computed with ICA and 3D. Since the near nadir radiances contribute more to the reflected irradiance than oblique radiances, above results suggest that the difference of the ICA irradiance from 3D irradiance is positive when the solar zenith angle is small. This is consistent with the result by *Davis and Marshak* [2001]. Our result also suggests that the irradiance difference decreases with solar zenith angle, which is consistent with that of *Chambers et al.* [1997] and *Benner and Evans* [2001].

[28] The above results (4) and (5) are on the RMS difference of r_{ICA} and r_{3D}. The optical thickness along the path of the direct solar irradiance in 3D and ICA computations are the same for overhead sun. The difference in the optical thickness along the path of the direct irradiance increases with solar zenith angle, which also increases the RMS $r_{ICA} - r_{3D}$ difference. Increasing RMS $r_{ICA} - r_{3D}$ difference with viewing angle is also due to a similar reason; the optical thicknesses along the line of sight in 3D and ICA computations agree at nadir but the difference increases with viewing zenith angle. The larger RMS $r_{ICA} - r_{3D}$ difference in the forward direction especially at the viewing zenith angle of 60 for large solar zenith angles is caused by the fact that the imager detects more transmitted photons at this angle in the 3D calculation than any other simulated viewing angles while the imager detects reflected photons in the ICA calculation. In the forward direction, therefore, the difference of the sensitivity to the optical thickness for reflected and transmitted photons, in addition to the difference in the optical thickness along the path, increases the RMS difference.

5. Error in the Retrieved Cloud Optical Thickness

[29] Figure 4 shows the error in the retrieved optical thickness $\overline{\Delta\tau}$ ($=\overline{\Delta\tau_e} + \overline{\Delta\tau_i}$) and error in the retrieved shape parameter ν of a gamma distribution as a function of relative azimuth angle. Note that a gamma distribution $P(\tau)$ of the optical thickness τ is expressed as

$$P(\tau) = \frac{1}{\Gamma(\nu)}\left(\frac{\nu}{\bar{\tau}}\right)^{\nu}\tau^{\nu-1}e^{-\nu\tau/\bar{\tau}}, \tag{5}$$

where $\Gamma(\nu)$ is the gamma function. The shape parameter is derived from linear and logarithmic mean of optical thicknesses [*Wilks*, 1995]. We also plot two terms $\overline{\Delta\tau_e}$ and $\overline{\Delta\tau_i}$ separately in Figures 5 and 6. Figure 5 shows the error in the retrieved optical thickness as a function of solar zenith angle separated by viewing zenith angle and Figure 6 shows the error as a function of relative azimuth angle separated by the solar zenith angle. On the basis of (3), the dependence of $\overline{\Delta\tau_e}$ on solar zenith, viewing zenith, and azimuth angles should be consistent with that of the $\overline{r_{ICA}} - \overline{r_{3D}}$ difference with the opposite sign. Increasing $\overline{\Delta\tau_e}$ with solar zenith angle when the viewing zenith angle is 0° or 30° (Figure 5) agrees with the result of decreasing the $\overline{r_{ICA}} - \overline{r_{3D}}$ difference. However, $\overline{\Delta\tau_e}$ is large positive when the viewing zenith angle is 60° and solar zenith angle is 70° (Figure 5). When the solar zenith angle is large, the reflectance at edges of the cloud top can be very large [*Evans and Marshak*, 2005]. The reflectance, as a function of optical thickness, approaches an asymptote value and

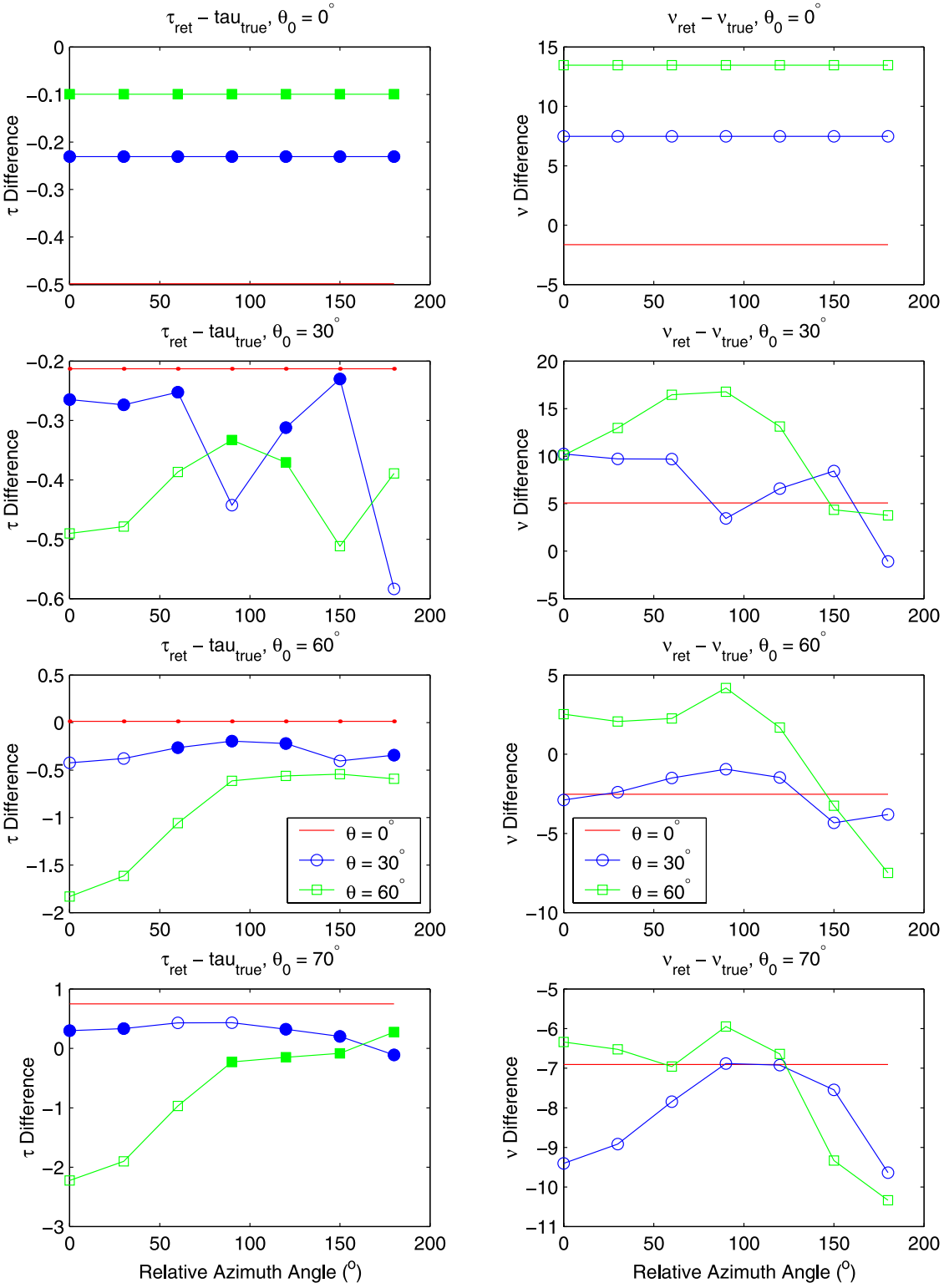

Figure 4. (left) Difference of the domain-averaged retrieved optical thickness and the true domain-averaged optical thickness ($\overline{\tau_{ret}} - \overline{\tau_{true}} = \overline{\Delta\tau}$). The relative azimuth angle is 0 when the imager looks into the sun. Optical thicknesses are retrieved with 1-km pixels. Solid lines indicate nadir view and lines with open circles and squares indicate, respectively, the viewing zenith angle of 30° and 60°. Solid symbols indicate the relative error less than 10%. The solar zenith angle increases from the top to bottom row (0°, 30°, 60°, and 70°). (right) Difference of the retrieved gamma distribution shape parameter and true shape parameter ($\nu_{\text{ret}} - \nu_{\text{true}}$). $\overline{\tau_{true}} = 3.75$ and $\overline{\nu_{true}} = 15$.

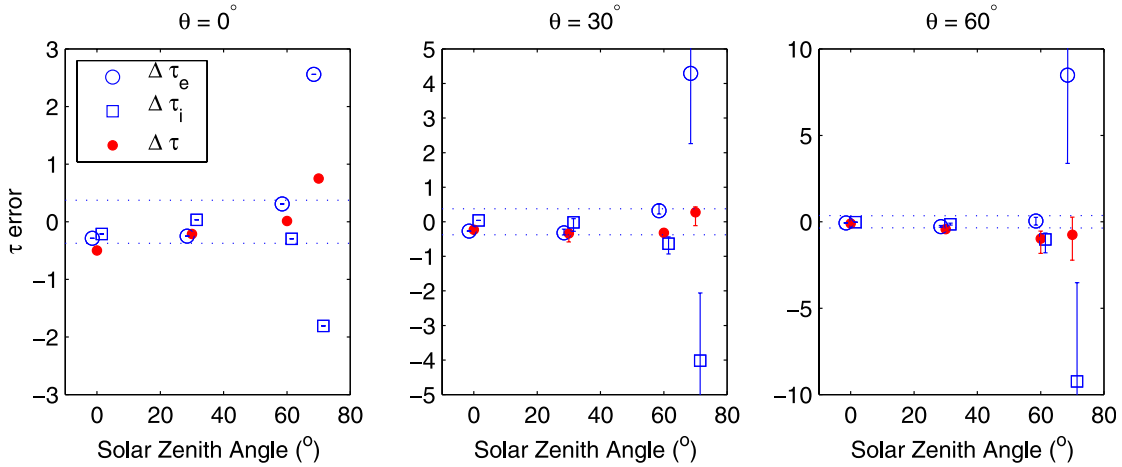

Figure 5. Domain-averaged retrieved optical thickness error $\overline{\Delta\tau} = \overline{\Delta\tau_i} + \overline{\Delta\tau_e}$ as a function of solar zenith angle (closed circles). Open circles and squares are plotted by slightly offsetting the solar zenith angle to allow easier distinction. Open circles indicate the error due to external variability $\overline{\Delta\tau_e}$, and open squares indicate the error due to neglecting horizontal inhomogeneity within 1-km imager pixels $\overline{\Delta\tau_i}$ (internal variability). Error bars indicate the maximum and minimum errors among all simulated relative azimuth angles. Horizontal dotted lines indicate the plus and minus 10% errors.

becomes nearly constant as the optical thickness increases. When the solar zenith angle is large, the reflectance asymptotes at smaller optical thickness than the reflectance for a smaller solar zenith angle does. As a consequence, it needs a large optical thickness to match a radiance observed in the forward direction at a large solar zenith angle with the radiance from 1D theory, if the forward reflectance peak is larger than that given by 1D theory. In our simulation, some retrieved optical thicknesses are greater than 100 (Figure 7). These large retrieved optical thicknesses increase the domain-averaged retrieved optical thickness. Because $\overline{\Delta\tau_e}$ represents the error in the domain-averaged optical thickness retrieved at a 50 m resolution, the result indicates that increasing the resolution increases the domain-averaged optical thickness error when the solar zenith angle is large. Figure 7 also shows that significant pixels have a small retrieved optical thickness error when the reflectance difference is negative. This is apparently caused by the forward peak of optically thinner columns because the radiance sensitivity to the optical thickness exists so that the 3D radiance can be matched with the ICA radiance by a small change of the optical thickness.

[30] The internal variability term $\Delta\tau_i$ is the error due to unresolved variability within a 1-km pixel. It follows from (4) that the retrieved optical thickness is negatively biased because the size of a pixel is finite (1 km in this simulation) and optical thickness to match the 1-km resolution radiance is smaller than a linear mean of optical thicknesses in the pixel. An extreme case of this is a pixel that is partially filled with clouds. The optical thickness retrieved from a partially filled pixel is also smaller than the true optical thickness [e.g., *Coakley et al.*, 2005]. Therefore $\Delta\tau_i$ is generally negative. However, when the cloud optical thickness is small, the derivative of reflectance with respect to the optical thickness decreases with decreasing the optical thickness and the reflectance function $r(\tau)$ is concave rather than convex. Figure 8 shows the derivative computed by DISORT [*Stamnes et al.*, 1988] with a plane parallel nonabsorbing clouds for overhead sun. The exact optical thickness at which the reflectance function becomes concave depends on solar zenith and viewing zenith angles. This means that $\overline{\Delta\tau_i}$ can be positive if clouds are optically thin. In Figure 6, the vertical error bar on $\overline{\Delta\tau_i}$ indicates that this happens in our simulation when the solar zenith angle is 0° and 30°, although $\overline{\Delta\tau_i}$ averaged over all viewing angles is negative. $\overline{\Delta\tau_i}$ becomes more negative as the solar zenith angle increases because clouds look more inhomogeneous. This is apparent in Figure 4 showing that the retrieved shape parameter of a gamma distribution decreases as the solar zenith angle increases (i.e., from top row to bottom row on the right column). Note that the shape parameter is equal to the square of the mean over standard deviation, which increases with decreasing standard deviation.

[31] In summary, the magnitude of $\overline{\Delta\tau_e}$ and $\overline{\Delta\tau_i}$ increases with solar zenith angle. They, however, tend to have opposite signs so that the error can partially cancel (Figures 5 and 6). Both terms are originated from horizontal inhomogeneity and the magnitude decreases as horizontal inhomogeneity decreases. However, $\Delta\tau_e$ and $\Delta\tau_i$ are caused by different assumptions in the retrieval process. The assumption of a uniform overcast cloud inside a pixel results in $\Delta\tau_i$ while neglecting horizontal flux causes $\Delta\tau_e$. The magnitude of both terms depends on the degree of inhomogeneity, the shape of reflectance function, and the size of pixel, but $\Delta\tau_e$ and $\Delta\tau_i$ have different dependence to them. $\Delta\tau_i$ is generally negative but can be also positive for a very small optical thickness. $\Delta\tau_i$ can be negligibly small if the pixel size decreases but the magnitude of $\Delta\tau_e$ increases with decreasing pixel size [e.g., *Davis et al.*, 1997]. $\overline{\Delta\tau_e}$ changes the sign from negative to positive as the solar zenith angle increases. A large positive $\overline{\Delta\tau_e}$ for $\theta = 60°$ and $\theta_0 = 70°$ is due to some large retrieved values at cloud top edges and the fact that reflectance function approaches an asymptote value at a smaller optical thickness when the solar zenith

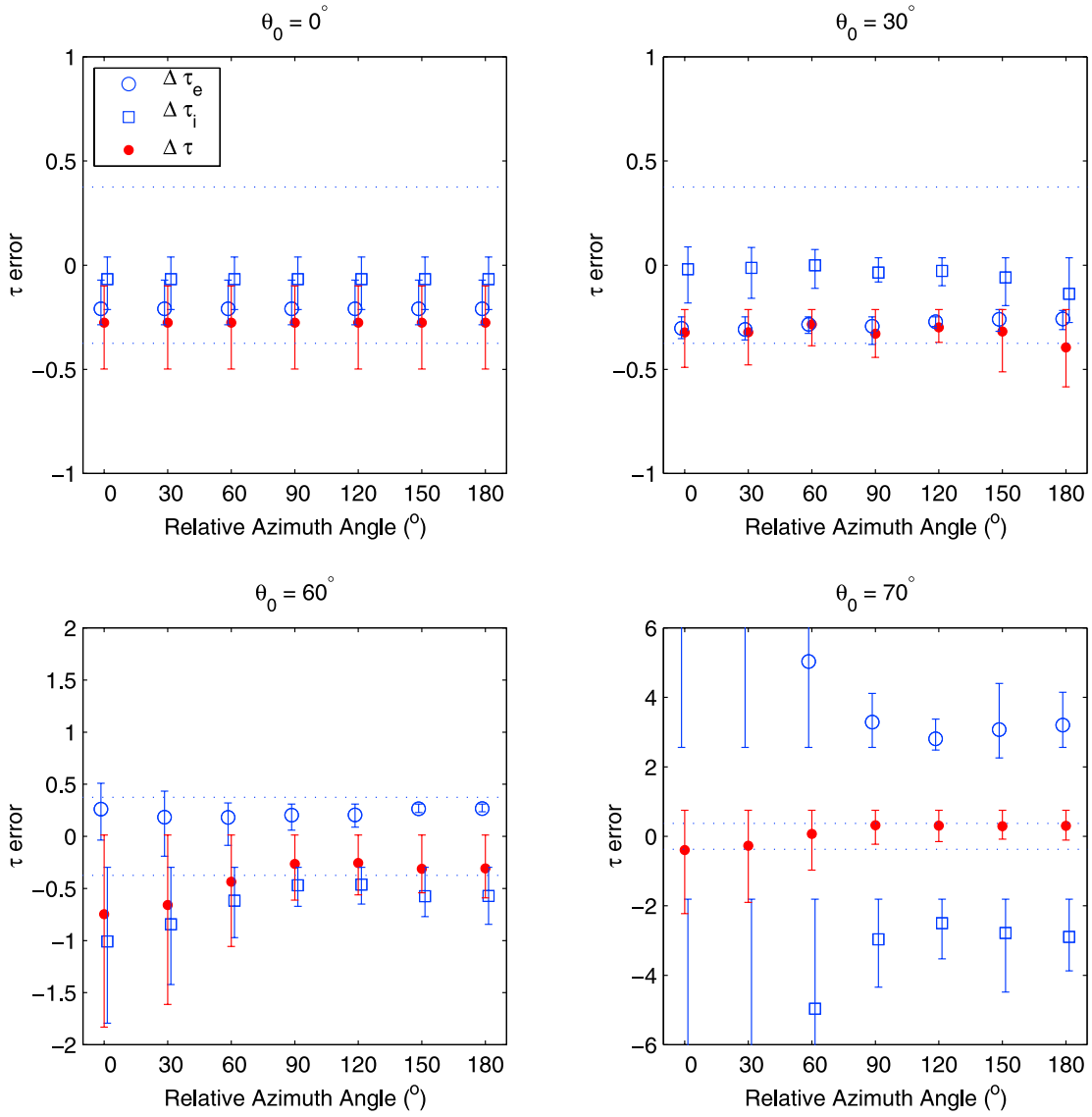

Figure 6. Domain-averaged retrieved optical thickness error $\overline{\Delta\tau}$ as a function of solar zenith angle (closed circles). Open circles indicate the error due to the subpixel-scale external variability $\overline{\Delta\tau_e}$, and open squares indicate the error due to neglecting horizontal inhomogeneity within 1-km imager pixels $\overline{\Delta\tau_i}$ (internal variability). Error bars indicate the maximum and minimum errors among all simulated viewing zenith angles. Horizontal dotted lines indicate the plus and minus 10% errors.

angle is large. Increasing $\overline{\Delta\tau_e}$ with solar zenith angle for $\theta = 0°$ and 30° is due to decreasing $r_{ICA} - r_{3D}$ with solar zenith angle, which is caused by the nature of the ICA that tends to increase the number of scattering events.

6. Optimum Viewing Geometry and Solar Zenith Angle

[32] On the basis of the result discussed above, we seek optimal viewing geometries and solar zenith angles that give a small $\overline{\Delta\tau}$. To determine whether or not $\overline{\Delta\tau}$ is sufficiently small, we use a 10% criterion of the optical thickness error required for climate data [*Ohring et al.*, 2005]. At a smaller solar zenith angle, both $\overline{\Delta\tau_e}$ and $\overline{\Delta\tau_i}$ terms derived from the cloud field used in our simulation are small (Figures 5 and 6). As a consequence, when the solar zenith angle is small ($\theta_0 \leq 30°$), the error is negative but less than 10% (except for $\phi = 180°$) for the cloud field we analyzed (Figure 6). However, if the optical thickness is derived from nadir view only for overhead sun, the domain-averaged optical thickness is underestimated by more than 10% (Figure 5). The azimuthally averaged $\overline{\Delta\tau}$ is less than 10% in the range of the viewing zenith angle from 0° to 60° when the solar zenith angle is around 30° (Figure 5). When the solar zenith angle increases to 60°, viewing zenith averaged $\overline{\Delta\tau}$ (closed circle) exceeds 10% especially if viewed from the forward direction while it can be less than 10% in the backward direction (Figure 6). The azimuthally averaged $\overline{\Delta\tau}$ is less than 10% when the viewing zenith angle is less than 30° and solar zenith angle is 60. When the solar zenith angle further increases to 70°, both terms are greater than 10% but with the opposite sign (Figures 5 and

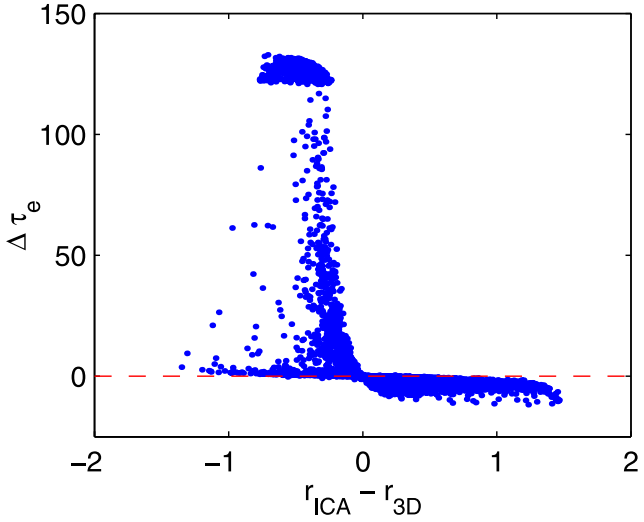

Figure 7. The error in the optical thickness retrieved from a 50-km pixel resolution $\Delta\tau_e$ as a function of the difference between ICA and 3D reflectances computed also with a 50-km resolution. The solar zenith angle is 70°, viewing and relative azimuth angles are 60° and 0°, respectively.

6). As a consequence, the optical thickness error retrieved from the cloud field used in our study is less than 10%. In the forward direction, for example, $\overline{\Delta\tau}$ is smaller when θ_0 is 70° than $\overline{\Delta\tau}$ when θ_0 is 60°. Because the small error is achieved by two large terms with the opposite sign when solar zenith angle is 70°, $\overline{\Delta\tau}$ at a large solar zenith angle possibly highly depends on the cloud field.

[33] We check whether or not this optimal viewing geometry and solar zenith angle combination can actually occur in the data taken from MODIS on Terra where low-level stratocumulus clouds are often present. Figure 9 shows the frequency of occurrence of viewing zenith and relative azimuth angles of MODIS and solar zenith angle over a 1° × 1° region centered at 32.5N and 134.5W. The solar zenith angle centered at about 30° occur in March and September. Since the viewing zenith angle is nearly uniformly distributed from 0° to 60°, we refer to Figure 6 for the domain-averaged optical thickness error. Figure 6 indicates that the errors are likely to be less than 10% in March and September when the solar zenith angle is near 30° and relative azimuth angles near 60° and 140° are sampled. The relative azimuth angle close to 0° occurs in June but the solar zenith angle is small so that the error in the forward direction is likely to be less than 10%. A larger error is possible in December when the solar zenith angle is about 60° and the relative azimuth angle is about 60°.

[34] As mentioned earlier, $\overline{\Delta\tau}$ discussed here is for relatively uniform water clouds. One could filter out highly inhomogeneous cloud fields using the shape parameter of a gamma distribution derived from subsets of optical thickness over a similar size of domain used in this study. The true shape parameter for the 3.4 km × 3.4 km cloud field used in this study computed with a 1-km resolution is 15. The retrieved shape parameter averaged over all simulated viewing geometries and solar zenith angle is 18 and the retrieved cloud cover with 1-km pixel is 100%. Therefore the result obtained in this study is applicable for a domain average computed from relatively uniform overcast clouds of which retrieved shape parameter is greater than about 15. Although we only studied one isotropic cloud field and whether or not the result can be extrapolated to uniform marine stratocumulus clouds is an open question, we simulated more than 9000 (4500 for nadir) 1 km optical thickness retrievals for a given viewing geometry and solar zenith angle. The above result indicates that the error in the domain-averaged retrieved optical thickness of uniform stratocumulus over northeastern Pacific is less than 10% in March and September when the solar zenith angle is around 30°.

[35] To investigate cloud properties similar to those used in this simulation actually happens under similar viewing geometry and solar zenith angle, we sort low-level clouds (cloud top height greater than 680 hPa) derived from observed MODIS radiances by the Clouds and the Earth's Radiant Energy System (CERES) cloud algorithm [*Minnis et al.*, 1998; *Minnis et al.*, 2008] over 134°W to 135°W and 30°N to 35°N as a function of retrieved optical thickness and shape parameter (Figure 10). The shape parameter is derived from linear and logarithmic mean of optical thicknesses derived over a CERES footprint, which is approximately 20 km at nadir, with 1 km MODIS pixels [*Kato et al.*, 2005]. Note that the actual MODIS pixel size increases with viewing zenith angle while it is constant in our simulation. Note also that the shape parameter depends on the domain size. As the domain size increases, the cloud optical thickness tends to be more variable, which reduces the shape parameter. Because a 20 km CERES footprint is larger than the domain used in the study, we expect that the shape parameter would be slightly larger if the CERES footprint size is smaller. When the solar zenith angle is 30° and the relative azimuth angle is 60° or 120° as sampled by

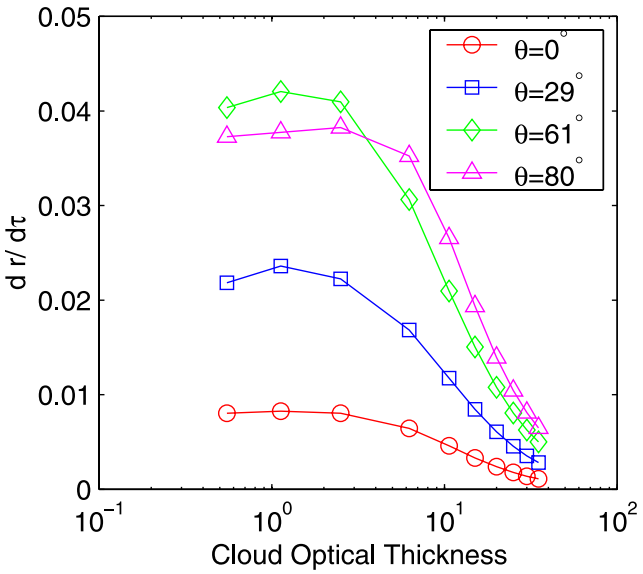

Figure 8. Derivative of the reflectance at 528 nm with respect to optical thickness as a function of optical thickness at 4 indicated viewing zenith angles. The derivative is computed for overhead sun with a plane parallel non-absorbing cloud of which cloud top is 3 km that is placed in the mid-latitude summer atmosphere.

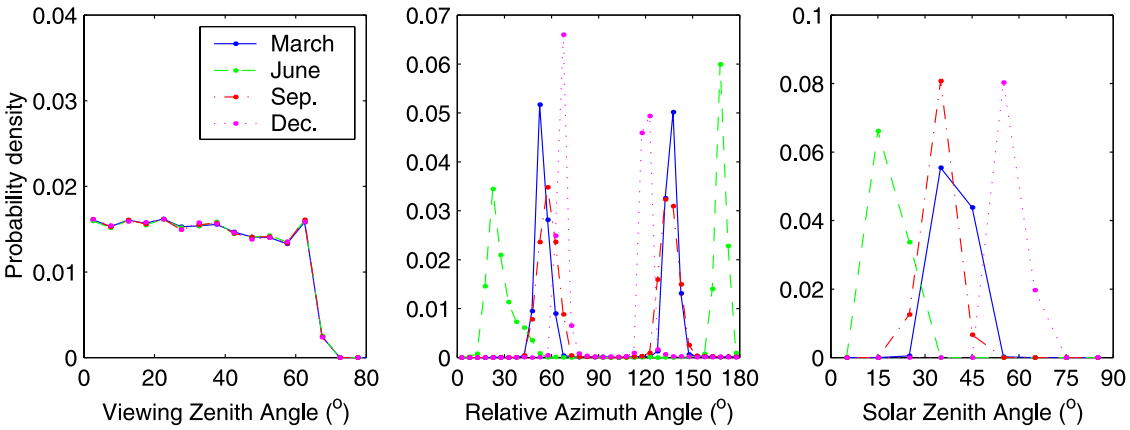

Figure 9. Probability of occurrence of viewing zenith and relative azimuth angles of MODIS on Terra, as well as probability of occurrence of the solar zenith angle at the time of the MODIS observation took place. Data are collected over a 1° × 1° region centered at 32.5°N and 134.5°W.

MODIS in March and September, the retrieved domain-averaged optical thickness from the cloud field used in this study is 3.4 and retrieved shape parameter from linear and logarithmic mean of retrieved optical thicknesses is 27 if they are averaged over all viewing zenith angles. Figure 10 indicates that the optical thickness and shape parameter used in this study actually occur, although the mode of the distribution is shifted toward optically thicker and less uniform clouds. Therefore, if we limit the domain-averaged retrieved cloud optical thickness and shape parameter to a similar range of those from the cloud field and if they show a similar, viewing, relative azimuth, and solar zenith angle dependence to those studied in this study, the retrieval error is likely to be less than 10%. A potential critical issue is that averaged cloud fields need to be nearly isotropic. Therefore a significant amount of retrieved optical thicknesses needs to be averaged.

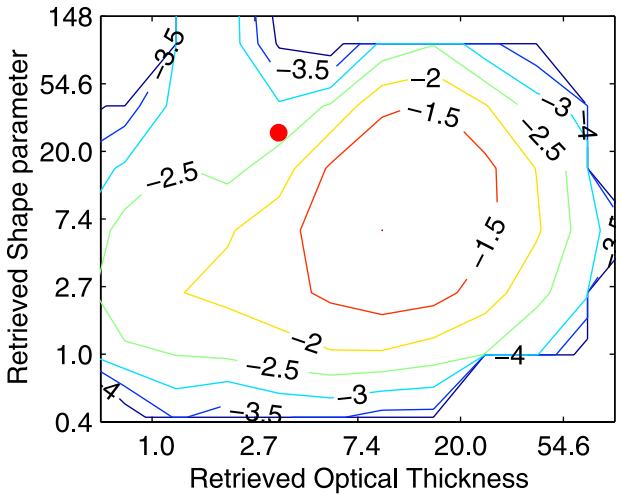

Figure 10. 2D histogram of cloud properties derived from 1-km MODIS pixels over CERES footprints between 134°W and 135°W and 30°N and 35°N in March 2003. The shape parameter of a gamma distribution is derived from the difference between linear and logarithmic mean of optical thicknesses [*Kato et al.*, 2005]. Contour is the logarithmic (base 10) of the number of samples. The closed circle indicates properties of the cloud field used in this study.

[36] Because the error depends on season and region (solar zenith angle), separating seasonal variation of cloud optical thickness is critical to understand the error in the retrieved optical thickness. While earlier studies simulate the retrieval process with a broader range of cloud properties [e.g., *Kato et al.*, 2006], we also need to extend simulations to optically thicker and less uniform clouds in future to broaden the cloud type for estimating the error in domain-averaged retrieved cloud optical thicknesses. In addition, we can compare the modeled TOA irradiance with these relatively uniform clouds and the irradiance derived from CERES radiances by angular distribution models to check a consistency, although calibration of MODIS and CERES instruments affect the result of this kind of comparisons.

7. Conclusions

[37] We investigated the error in the retrieved cloud optical thickness as a function of viewing zenith, relative azimuth, and solar zenith angles for a relatively uniform cloud field. The retrieved cloud fraction with 1-km pixels is 1 and the retrieved shape parameter averaged over all simulated solar zenith angle is 18 while the true values are 3.75 and 15, respectively. The error in the retrieved optical thickness is separated into two terms, the error due to external variability $\overline{\Delta\tau_e}$ and the error due to internal variability $\overline{\Delta\tau_i}$. $\overline{\Delta\tau_e}$ is caused by the independent column approximation applied to subpixels and $\overline{\Delta\tau_i}$ caused by the assumption of a uniform overcast clouds within a 1-km pixel. We determine the optimal viewing geometry and solar zenith angle that give less than 10% error of the domain-averaged retrieved optical thickness from the cloud field used in the simulation. When the solar zenith angle is small (less than ≈30°), the azimuthally averaged $\overline{\Delta\tau}$ is most likely less than 10%. In addition, the $\overline{\Delta\tau}$ averaged over viewing zenith angle is less than 10% when optical thicknesses are derived from the relative azimuth angle smaller than ≈150°. However, if the optical thickness is derived from nadir view only for overhead sun, the domain-averaged optical thickness is underestimated by more than 10%. When the solar zenith angle increases to 60°, the viewing

zenith angle averaged $\overline{\Delta\tau}$ is also likely to be less than 10% in the backward direction. The azimuthally averaged $\overline{\Delta\tau}$ is also likely to be less than 10% if viewing zenith angle is small (less than $\approx 30°$) but exceeds 10% for large viewing zenith angles (greater than $\approx 60°$). The viewing zenith angle averaged $\overline{\Delta\tau}$ also exceeds 10% in the forward direction. When the solar zenith angle is further increased to 70°, both terms $\overline{\Delta\tau_e}$ and $\overline{\Delta\tau_e}$ are greater than 10% with the opposite sign so that $\overline{\Delta\tau}$ is smaller, although the magnitude of $\overline{\Delta\tau}$ possibly highly depends on cloud field. We checked MODIS viewing geometry from *Terra* satellite and showed that the optimal viewing geometry over northeastern pacific where low-level stratocumulus clouds are often present actually happens. We expect the domain-averaged error in MODIS retrieved cloud optical thickness from cloud fields similar to the cloud field used in this study to be less than 10%, if retrieved optical thicknesses show a similar viewing angle and solar zenith angle dependence when a significant amount of optical thicknesses are averaged.

[38] **Acknowledgments.** We are grateful to F. Evans for providing SHDOM and Lazaros Oreopoulos and two anonymous reviewers for constructive comments. This work was supported by NASA through the Clouds and the Earth's Radiant Energy System (CERES) project and the radiation science program.

References

Aronson, R. (1997), Radiative transfer implies a modified reciprocity relation, *J. Opt. Soc. Am. A*, *14*, 486–490.

Benner, T. C., and K. F. Evans (2001), Three-dimensional solar radiative transfer in small tropical cumulus fields derived from high-resolution imagery, *J. Geophys. Res.*, *106*(D14), 14,975–14,984.

Cahalan, R. F., W. Ridgway, W. J. Wiscombe, S. Gollmer, and Harshvardhan (1994), Independent pixel and Monte Carlo estimates of stratocumulus albedo, *J. Atmos. Sci.*, *51*, 3776–3790.

Chambers, L. H., B. A. Wielicki, and K. F. Evans (1997), Independent pixel and two-dimensional estimates of Landsat-derived cloud field albedo, *J. Atmos. Sci.*, *54*, 1525–1532.

Coakley, J. A., M. A. Friedman, and W. R. Tahnk (2005), Retrieval of cloud properties for partly cloudy imager pixels, *J. Atmos. Oceanic Technol.*, *22*, 3–17.

Davies, R. (1994), Spatial autocorrelation of radiation measured by the Earth Radiation Budget Experiment: Science inhomogeneity and reciprocity violation, *J. Geophys. Res.*, *99*, 20,879–20,887.

Davis, A., and Y. Knyazikhin (2005), A primer in 3D radiative transfer, in *Three-Dimensional Radiative Transfer in Cloudy Atmospheres*, edited by A. Marshak and A. B. Davis, pp. 153–242, Springer, New York.

Davis, A. B., and A. Marshak (2001), Multiple scattering in clouds: Insights from three-dimensional diffusion/P_1 theory, *Nucl. Sci. Eng.*, *137*, 251–280.

Davis, A., A. Marshak, R. Cahalan, and W. Wiscombe (1997), The Landsat scale brake in stratocumulus as a three-dimensional radiative transfer effect: Implication for cloud remote sensing, *J. Atmos. Sci.*, *54*, 241–260.

Di Girolamo, L. (2002), Reciprocity principle for radiative transfer models that use periodic boundary conditions, *J. Quant. Spectrosc. Radiat. Transfer*, *73*, 23–27.

Di Girolamo, T. Várnai, and R. Davies (1998), Apparent breakdown of reciprocity in reflected solar radiances, *J. Geophys. Res.*, *103*(D8), 8795–8803.

Dong, X., P. Minnis, B. Xi, S. Sun-Mack, and Y. Chen (2008), Comparison of CERES-MODIS stratus cloud properties with ground-based measurements at the DOE ARM Southern Great Plains site, *J. Geophys. Res.*, *113*, D03204, doi:10.1029/2007JD008438.

Evans, K. F. (1998), The spherical harmonic discrete ordinate method for three-dimensional atmospheric radiative transfer, *J. Atmos. Sci.*, *55*, 429–446.

Evans, K. F., and A. Marshak (2005), Numerical methods, in *Three-Dimensional Radiative Transfer in Cloudy Atmosphere*, edited by A. Marshak and A. B. Davis, pp. 243–281, Springer, New York.

Hinkelman, L. M., B. Stevens, and K. F. Evans (2005), A large-eddy simulation study of anisotropy in fair-weather cumulus cloud fields, *J. Atmos. Sci.*, *62*, 2155–2171.

Kato, S., F. G. Rose, and T. P. Charlock (2005), Computation of domain-averaged irradiance using satellite-derived cloud properties, *J. Atmos. Oceanic Technol.*, *22*, 146–164.

Kato, S., L. M. Hinkelman, and A. Cheng (2006), Estimate of satellite-derived cloud optical thickness and effective radius errors and their effect on computed domain-averaged irradiances, *J. Geophys. Res.*, *111*, D17201, doi:10.1029/2005JD006668.

King, M. D., Y. J. Kaufman, W. P. Menzel, and D. Tanre (1992), Remote sensing of cloud, aerosol, and water vapor properties from the Moderate Resolution Imaging Spectrometer (MODIS), *IEEE Trans. Geosci. Remote Sens.*, *30*, 2–27.

Loeb, N. G., and J. A. Coakley Jr. (1998), Influence of marine stratus cloud optical depth from satellite measurements: Does 1D theory apply?, *J. Clim.*, *11*, 215–233.

Loeb, N. G., T. Várnai, and R. Davies (1997), Effect of cloud inhomogeneities on the solar zenith angle dependence of nadir reflectance, *J. Geophys. Res.*, *112*(D8), 9387–9395.

Loeb, N. G., T. Várnai, and D. M. Winker (1998), Influence of subpixel-scale cloud-top structure on reflectance from overcast stratiform cloud layers, *J. Atmos. Sci.*, *55*, 2960–2973.

Loeb, N. G., B. A. Wielicki, W. Su, K. Loukachine, W. Sun, T. Wong, K. J. Priestley, G. Mathews, W. F. Miller, and R. Davies (2007), Multi-instrument comparison of top-of-atmosphere reflected solar radiation, *J. Clim.*, *20*, 575–591.

Mace, G. G., Y. Zhang, S. Platnick, M. D. King, P. Minnis, and P. Yang (2005), Evaluation of cirrus cloud properties from MODIS radiances using cloud properties derived from ground-based data collected at the ARM SGP site, *J. Appl. Meteorol.*, *44*, 221–240.

Marshak, A., A. B. Davis, W. Wiscombe, and R. Cahalan (1995), Radiative smoothing in fractal clouds, *J. Geophys. Res.*, *100*(D12), 26,247–26,261.

Marshak, A., S. Platnick, T. Várnai, G. Wen, and R. F. Cahalan (2006), Impact of 3D radiative effects on satellite retrievals of cloud droplet sizes, *J. Geophys. Res.*, *111*, D09207, doi:10.1029/2005JD006686.

Minnis, P., D. P. Garber, D. F. Young, R. F. Arduni, and Y. Takano (1998), Parameterization of reflectance and effective emittance for satellite remote sensing of cloud properties, *J. Atmos. Sci.*, *55*, 3313–3339.

Minnis, P., et al. (2008), Cloud detection in non-polar regions for CERES using TRMM VIRS and Terra and Aqua MODIS data, *IEEE Trans. Geosci. Remote Sens.*, *46*, 3857–3884.

Ohring, G., B. Wielicki, R. Spencer, B. Emery, and R. Datla (2005), Satellite instrument calibration for measuring global climate change, *Bull. Am. Meteorol. Soc.*, *86*, 1303–1313.

Platnick, S., J. Y. Li, M. D. King, H. Gerber, and P. V. Hobbs (2001), A solar reflectance method for retrieving the optical thickness and droplet size of liquid water clouds over snow and ice surface, *J. Geophys. Res.*, *106*(D14), 15,185–15,199.

Ramanathan, V. R. D., E. F. Cess, P. Harrison, B. Minnis, R. Barkstrom, E. Ahmad, and D. Hartmann (1989), Cloud-radiative forcing and climate: Results from the earth radiation budget experiment, *Science*, *243*, 57–63.

Stamnes, K., S.-C. Tsay, W. Wiscombe, and K. Jayaweera (1988), Numerically stable algorithm for discrete-ordinate-method radiative transfer in multiple scattering and emitting layered media, *Appl. Opt.*, *27*, 2502–2509.

Stevens, B., C.-H. Moeng, and P. P. Sullivan (1999), Large-eddy simulation of radiatively driven convection: Sensitivities to the representation of small scales, *J. Atmos. Sci.*, *56*, 3963–3984.

Várnai, T., and A. Marshak (2003), A method for analyzing how various parts of clouds influence each other's brightness, *J. Geophys. Res.*, *108*(D22), 4706, doi:10.1029/2003JD003561.

Várnai, T., and A. Marshak (2007), View angle dependence of cloud optical thickness retrieved by Moderate Resolution Imaging Spectroradiometer (MODIS), *J. Geophys. Res.*, *112*, D06203, doi:10.1029/2005JD006912.

Wilks, D. S. (1995), *Statistical Methods in the Atmospheric Sciences*, 467 pp., Academic Press, New York.

Zinner, T., and B. Mayer (2006), Remote sensing of stratocumulus clouds: Uncertainties and biases due to inhomogeneity, *J. Geophys. Res.*, *111*, D14209, doi:10.1029/2005JD006955.

Zinner, T., B. Mayer, and M. Schröder (2006), Determination of three-dimensional cloud structures from high-resolution radiance data, *J. Geophys. Res.*, *111*, D08204, doi:10.1029/2005JD006062.

Zuidema, P., and K. F. Evans (1998), On the validity of the independent pixel approximation for boundary layer clouds observed during ASTEX, *J. Geophys. Res.*, *103*(D6), 6059–6074.

S. Kato, Climate Directorate, NASA Langley Research Center, MS 420, Hampton, VA 23681-2199, USA. (seiji.kato@nasa.gov)

A. Marshak, Climate and Radiation Branch, NASA Goddard Space Flight Center, Code 613.2, Greenbelt, MD 20771, USA. (Alexander.Marshak@nasa.gov)